ORIGINAL RESEARCH ARTICLE

In Situ Pre-heating in Wire Arc Additive Manufacturing: Design, Development, and Experimental Investigation on Residual Stresses and Metallurgical and Mechanical Properties

Neel Kamal Gupta, G. Ganesan (iD), S. Siddhartha, Shahu R. Karade, Arun Kumar Paul, Sudhanshu Dubey, Ronald H. Ely, and K.P. Karunakaran

Wire arc additive manufacturing (WAAM) employs an electric arc-based deposition process, but achieving the desired mechanical and metallurgical properties in WAAM is challenging. The pre-heating phase is critical for reducing residual stress and maintaining consistent heat input. This study introduces an automated induction-based pre-heating system integrated and made compatible with WAAM, evaluating its effectiveness on low carbon steel (ER 70S-6). The induction pre-heater is designed to meet application-specific needs, with dynamic power adjustments based on material composition and substrate size. It comprises a power source, cooling chiller, coil box, and pyrometer for temperature monitoring. Deposition is done using a CNC system utilizing a Cold Metal Transfer Metal Inert Gas (CMT-MIG) setup, comparing samples with and without pre-heating at maximum temperature. The study employs various techniques, including Electron Back-Scattered Diffraction analysis, x-ray diffraction, microhardness testing, and tensile tests, to assess the impact of pre-heating on dilution, grain size, residual stress, and mechanical properties. The results of this investigation illustrate that pre-heating markedly augments dilution by 15-20%, thereby fortifying interlayer bonding. Additionally, it refines the grain structure, diminishes residual stress by up to 50%, and elevates tensile strength by 10%, accompanied by an approximate 20% increase in hardness value for low carbon steel. The induction-based pre-heating system innovated in this research seamlessly integrates with Wire Arc Additive Manufacturing (WAAM), providing significant benefits in attaining the desired mechanical and metallurgical properties for additively manufactured components.

1. Introduction

1.1 Background

The process of adding material layer-by-layer to form a geometry is termed as Additive Manufacturing (AM). The most common energy source used in metal AM is *electric arc-based* deposition due to its high deposition rate (Ref 1, 2). The process is popularly termed as Wire Arc Additive Manufacturing (WAAM), which employs the material to deposit on a build plate called *substrate*. The process is now utilized to form a large component with various grades of materials (Ref 1, 3, 4). However, there are various challenges in WAAM that need to be comprehended for desired mechanical and metallurgical properties and minimizing the residual stresses which causes failure due to inadequate pre-heating.

Owing to temperature gradients induced by substantial heat input and recurrent thermal excursions, WAAM-fabricated specimens commonly harbor notable residual stress (Ref 5). This residual stress has the propensity to induce warpage or plastic deformation in components, potentially resulting in the occurrence of cracks or other defects (Ref 2, 6). Substrate pre-heating process is applied in WAAM for minimizing the thermal gradient which contributed to reduced Residual stress (Ref 7, 8).

Pre-heating is vital in AM to reduce thermal stress, prevent deformation, cracks, and maintains mechanical and metallurgical integrity with uniform heat input (Ref 9, 10). Substrate pre-heating in AM at various temperatures mitigates cracking and distortion issues due to more gradual thermal cycle and decrease in the molten pool's cooling rate (Ref 2, 11). Pre-heating also results in the high density of the deposited samples (Ref 10). The effect of pre-heating on different samples was attributed to more uniform grain structure compared to non pre-heating case; it was examined through electron back-scattered diffraction (EBSD) maps (Ref 12). The frequency of occurrence of columnar grain size is minimized by increasing pre-heating,

Neel Kamal Gupta, S. Siddhartha, Shahu R. Karade, Sudhanshu Dubey, Ronald H. Ely, and K.P. Karunakaran, Department of Mechanical Engineering, Indian Institute of Technology Bombay, Powai, Mumbai 400076, India; G. Ganesan, Department of Metallurgical Engineering and Materials Science, Indian Institute of Technology Bombay, Powai, Mumbai 400076, India; Arun Kumar Paul, Research and Development, M/S. Electronics Devices Worldwide Pvt. Ltd, 22 Mistry Industrial Estate, Cross Road A, Andheri East, Mumbai 400093, India. Contact e-mail: ganesangunasekaran01@gmail.com.

and it is due to a reduction in the thermal gradient (Ref 13). The dilution (also termed as penetration) increases when the substrate was pre-heated (Ref 14), while it reduces the height of the deposition due to gradual cooling rate post deposition. The dilution was enhanced by induction pre-heating of substrate to the temperature of 500 °C and deposition was carried by laser source which attributed to a higher absorption of the laser power (Ref 15). In another study by Boudreault et al. (Ref 16), an induction-based localized heating setup was proposed for repair work at small region only. A high frequency, flat spiral coil was utilized to control the temperature difference locally (Ref 17). This local based heating setup has challenges in terms of uniformity in temperature for the application of WAAM as the temperature at the start and end will vary due to movement of the system to cover the required area for deposition. Therefore, a system needs to designed and developed for the application of pre-heating in WAAM, uniformly across the deposition, to minimize the residual stress and improve the properties.

1.2 Challenges of Pre-heating in WAAM

Pre-heating in WAAM refers to the application of heat to the substrate or the workpiece before the actual additive manufacturing process begins. Various literature shows the benefits of pre-heating using different energy sources in welding/additive manufacturing areas such as Tungsten Inert Gas (TIG) arc, laser, and plasma with several experimental results (Ref 18-20). However, the problem still persists in the process of uniform pre-heating (Ref 21). Few of the major problems are energy consumption, uniformity in temperature, temperature measurement, process control, material compatibility, complex geometries, closed-loop feedback system, safety concerns, equipment complexity and many more (Ref 19). No pre-heating system can address all these challenges. Tackling these challenges requires integrating sophisticated process monitoring and control systems, optimizing materials, and meticulously assessing the unique demands of the printing application. Ongoing efforts by researchers and practitioners in the field focus on refining pre-heating techniques to elevate the overall performance and reliability of WAAM processes.

1.3 Need for Induction Pre-heater

There are various ways to do the pre-heating in WAAM; the adopted one should be energy and process efficient. Induction heating (Ref 22), with the ability of controlled power transfer contactless, removes the need for any pollutant energy source around the heating metal object; it makes the complete system compact and clean. Induction pre-heating is highly efficient because it directly heats the material through electromagnetic induction without any physical contact, the arrangement is compact as well (Ref 16, 19). The heat is generated within the material itself, minimizing heat loss to the surrounding. Induction heating is widely used in metal industry and it can achieve high heating rates, resulting in fast and uniform heating throughout the material when compared with other pre-heating techniques (Ref 16, 21). As there is no physical contact between the heating element and the material being heated, the process becomes more favorable for the WAAM, as it further improves the durability of the bounding box containing the coils. For transfer of desired heat, an induction-based pancake coil system is considered to be more efficient for horizontally

growing component in WAAM to pre-heat the substrate or the previously deposited layer.

In the context of WAAM, a challenge exists in achieving compatible pre-heating. This paper introduces an automated induction-based pre-heating system with a feedback loop integrated with the WAAM setup. Furthermore, the paper presents the design and development of a water cooled, pancake coil, induction-based pre-heating system and effectiveness of pre-heating through a series of experiments and study on residual stress, dilution, mechanical properties and microstructure refinement.

2. Experimental Setup

2.1 Design of Induction Pre-heater

The induction pre-heating system is desired to be engineered to facilitate pre-heating of substrates or previously deposited layers. Its design involves three major issues, they are:

1. The transferred energy should be efficiently utilized within the metal object for pre-heating purpose
2. The power controller needs to transfer the desired energy to the material efficiently, and
3. The designed system should be able to cater wide range of pre-heating applications

To utilize the transferred power efficiently, even for stress relieving applications, the design of an induction-heating system is application specific. The electromagnetic parameters of the metal object to be pre-heated define the characteristics of the pre-heating system. The transferred energy is concentrated on the surface whose depth δ is decided by skin effect, presented in Eq. (1),

$$\delta = \frac{1}{\sqrt{4\pi^2 \text{X} 10^{-7}}} \sqrt{\frac{\rho}{\mu_r f_s}} \qquad \text{(Eq 1)}$$

Where μ_r and ρ respectively are relative permeability and resistivity of the metal and f_s is the switching frequency of the inverter. Due to large value of μ_r, even at moderate f_s, the value of δ in soft iron is small. A material with high value of μ_r would need low-frequency inverter (see Fig. 1a, say, App-1), and non-magnetic materials may need high frequency system (say, App-3). The desired frequency is met by properly setting the resonant frequency f_r as shown in Eq. 2.

$$f_r = \frac{1}{2\pi\sqrt{(L_1 C_r)}} \qquad \text{(Eq 2)}$$

C_r is the capacitor of the tank circuit and L_1 is the inductance of coil head. The tank circuit capacitor C_r (see Fig. 1b) is used to improve the load power factor and it inherently assists the inverter for certain soft-switching. The transfer efficiency between the system and the metal object and how effectively the transferred power is utilized for stress relieving together would decide the energy efficiency. And, for control of heating profile accurately for wide range of objects, the controller needs to possess a fine power control feature (see Fig. 1b).

The coil L_1 facilitates the requisite energy transfer for pre-heating. The total power P_L transferred to the substrate depends on four parameters as presented in Eq. 3,
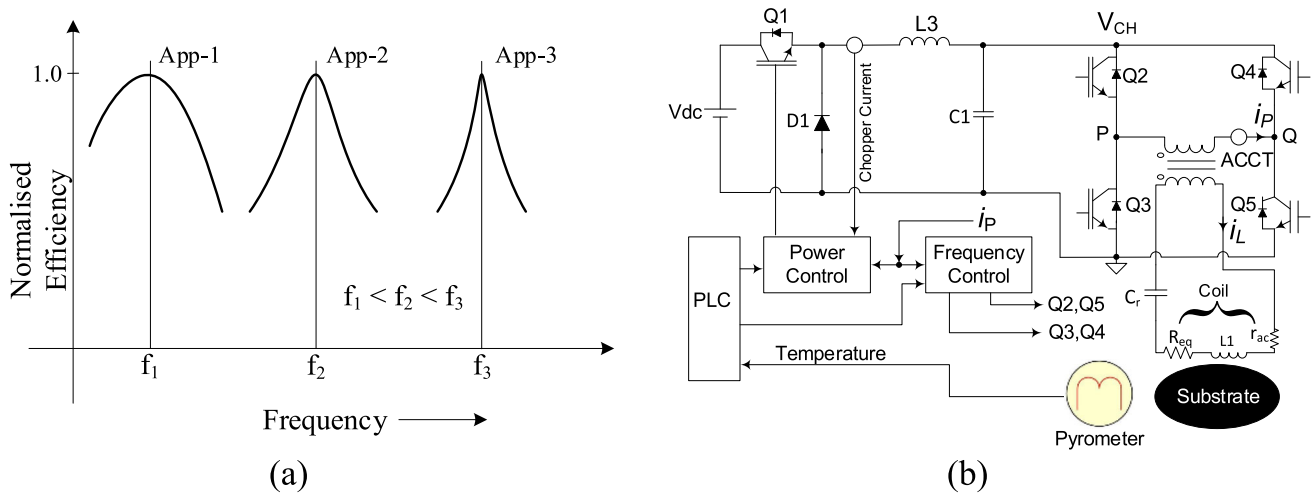
Fig. 1 (a) Role of frequency in induction-heating applications, and (b) Schematic diagram of induction-heating system

$$P_L = K_c L_1 i_L^2 f_s = i_L^2 R_{eq} \qquad \text{(Eq 3)}$$

L_1 is inductance of the coil head, i_L is current through it, f_s is the inverter frequency, i.e., the frequency of current i_L and the parameter K_c depends on coupling between the coil and the substrate. R_{eq} represents the total load resistance of the substrate reflected to the tank circuit. Large number of power converter configurations exists for energy transfer (Ref 23). For efficient energy transfer the inverter should operate close to the resonant condition. To cater wide range applications energy efficiently, series resonant inverter (see Fig. 1b) with zero voltage and near zero current switching (ZVZCS) topology is preferred (Ref 23). Considering for clarity that there is no loss by thermal radiation and convection, the transferred power P_L needed to raise the temperature of the substrate to, say, T °C from ambient T_{amb} (°C) in the pre-heating time duration t_{heat} could be expressed as shown in Eq. 2,

$$P_L = \frac{K_1 V_{CH}^2}{R_{eq}} = \frac{mC_p(T - T_{amb})}{t_{heat}} + P_w \qquad \text{(Eq 4)}$$

C_p is the specific heat, m is mass to be heated, chopper voltage V_{CH} is varied for power control, R_{eq} is the effective load resistance, the parameter K_1 includes coupling coefficient between L_1 and the heating object and P_w is the power wasted by convection and radiation. For a particular pre-heating applications with fixed R_{eq}, in ZVZCS inverter the transferred power P_L is accurately controlled by changing the value of V_{CH} (4).

Several factors influence the design of pre-heating system; a few of them are:

1. The system is equipped to operate at its maximum designed power capacity. Depending on the material composition and substrate size, the power demand automatically adjusts, resulting in variable power levels; it needs power control feature.
2. The heating duration depends on the surface area, with larger areas requiring efficient power distribution via a suitable coil. Thermal conductivity of the material also affects heating time, alongside the value of K_1.
3. An air gap impedes effective heating. Increasing the air gap reduces K_1, but raising the nominal frequency f can
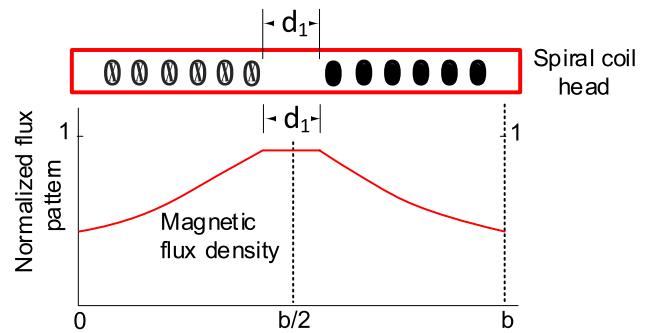

Fig. 2 Magnetic field distribution of a pancake coils for induction pre-heating system (b: coil diameter)

enhance it. A larger air gap delays efficient heating. A 10-mm gap between the coil box and substrate was maintained to prevent contact, ensuring the longevity of the glass fiber component.

The system is designed to take a job up to 500 mm diameter, and it is based on the properties of mild-steel however, it can pre-heat any metallic material with appropriate change in desired output temperature, pre-heating time and air gap. To meet this requirement, a 25-kW system was developed for this purpose, capable of achieving a temperature up to 400 °C within 120 seconds for mild-steel, even considering a 10-mm air gap. The addition of a power control block not only meets wide range of application prospects, it minimizes power loss because the inverter operates in ZVZCS conditions. The resonant frequency of the unloaded tank circuit was kept at 16 kHz.

For distribution of transferred power P_L over the surface area of the substrate spiral pancake coil (see Fig. 2) is preferred. The field distribution could be altered by changing the value of inner diameter or number of turns. Moreover, the magnetic coupling could be altered by adjusting the distance between the coil head and the substrate.
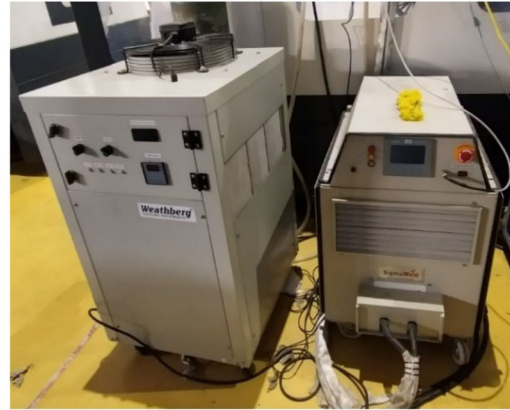
For the actual system water-cooled pancake coil (see Fig. 3a) was used because the current density ($\geq 10A/mm^2$) needed in L_1 was large, litz-wire-based air-cooled coil was not suitable. However, due to skin effect, large value of ac
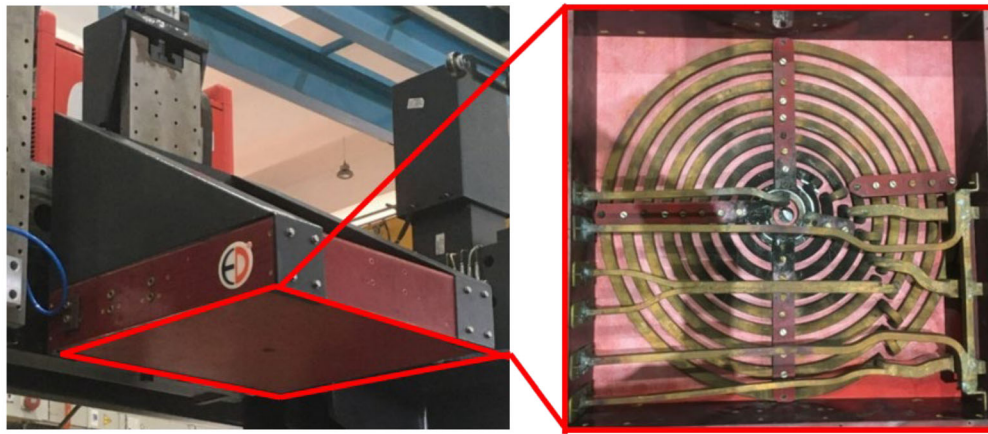
(a) Pan-cake coil
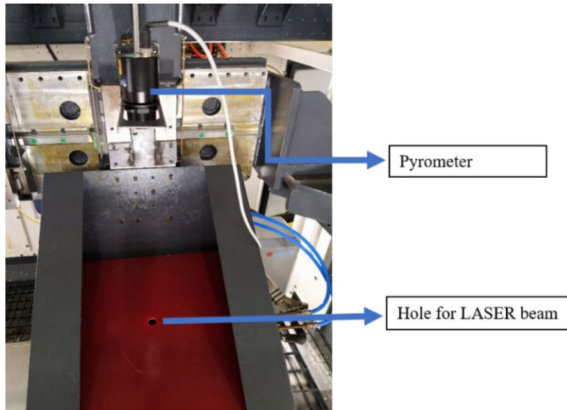
(b) Pyrometer for temperature sensing

(c) Chiller (left) and Controller (right) unit

Fig. 3 Induction-based pre-heating system

resistance r_{ac} of L_1 consisting of copper (Cu) tube would cause large power loss, necessitating a water-cooled design. This coil system can efficiently pre-heat materials with a diameter of up to 500 mm. The pre-heater setup consists of four key components: a power source, a chiller unit for coil cooling via water circulation, a coil box, and a pyrometer.

The 25 kW inverter is connected to the coil head L_1 via litz wire cable and is integrated with a chiller for effective cooling of L_1 and C_r, in particular. The laser-beam type pyrometer monitors the temperature and automatically terminates the heating process upon reaching the desired temperature, as illustrated in Fig. 3(b). The controller and chiller unit are presented in Fig. 3(c). Once the target temperature is achieved, the pre-heating process is cut-off automatically using a feedback loop controller of pre-heater which is interfaced with the controller of machine system where the deposition is carried out and the substrate-carrying platform advanced to the deposition station within the same machine.

Various benefits of the proposed system can be identified as:

1. Swift and uniform heating is achieved throughout the entire part or component.
2. The heating is specifically targeted to the top surface, extending up to 5 mm, ensuring minimal disruption to other layers.
3. A pyrometer is employed to continuously monitor the temperature in a closed-loop system, automatically ceasing operation once the desired temperature is achieved.

4. This method preserves the shape and size of the part, preventing alterations.
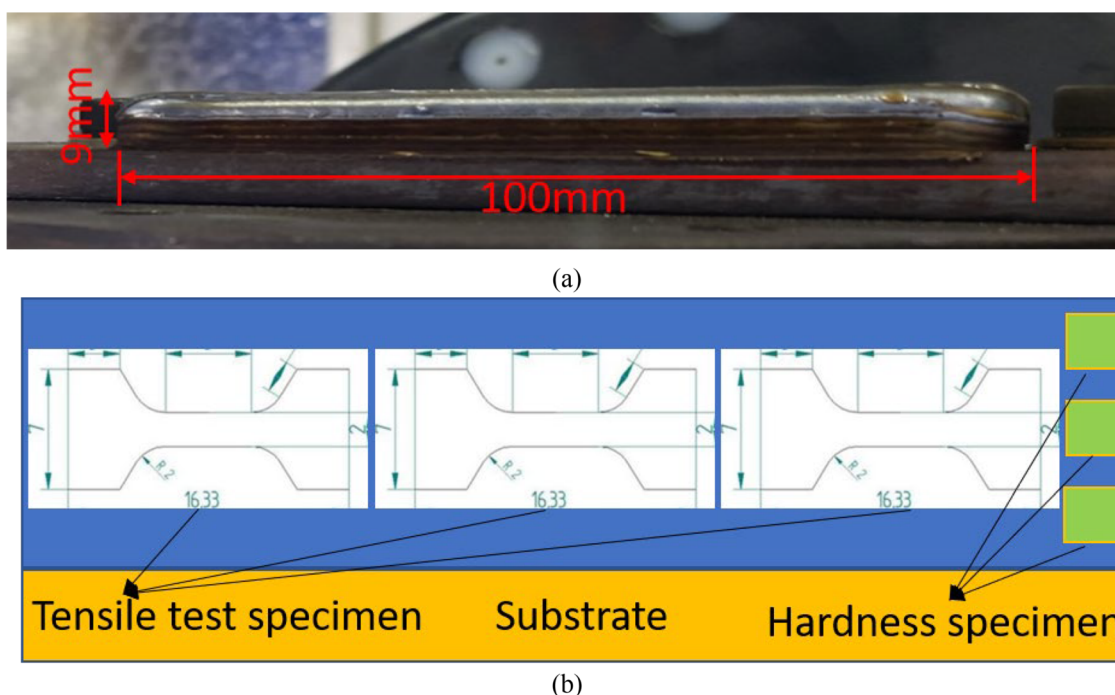
2.2 Deposition Setup

The deposition was carried out on a multi-platform CNC-based system using a CMT-MIG setup from Fronius with 1.2 mm wire diameter to deposit a 100 mm x 10 mm x 9 mm block using mild-steel material (ER70S-6). The deposition was carried on rolled mild-steel with low carbon content and thickness of plate was 10 mm. Material composition and deposition parameters are presented in Tables 1 & 2. Stepover is the overlap between the first pass and the second pass of deposition in multi-pass deposition, in this study the stepover was taken as 2 mm. Six layers, each of layer thickness 1.5 mm, were deposited, resulting in a 9 mm height as shown in Fig. 4(a). Each layer was face milled to a height of 1.5 mm, every time, and therefore the consistency of layer thickness of 1.5 mm was maintained throughout. Similar blocks were deposited without and with interlayer pre-heating, maintaining other parameters. The pre-heat temperature was 400 °C, and there was a marginal loss in the temperature at the time of deposition, maintaining the substrate near 350 °C. Fig. 4(b) presents the location for test scheme for tensile strength and microhardness. For the above practical demonstration, the parameters of the pre-heating systems are as follows: Coil inductance L_1:17 μH, water-cooled, Resonant capacitor C_r:6

Table 1 Composition of ER70S-6 material (in wt.%) (Ref 24)

Mn	Si	Cu	C	Ni	Cr	V	Mo	S	P	Fe
1.60	0.90	0.20	0.09	0.05	0.05	0.05	0.05	0.007	0.007	Balance

Table 2 Process parameters for deposition

Parameters	Current, A	Voltage, V	Stand-off-distance, mm	Gas flow rate, L/min	Feed, mm/min	Step over, mm
Values	100	22.5	12	15	800	2

(a)

(b)

Fig. 4 (a) Sample with multi-layer deposition; (b) Tensile and hardness test samples at various locations

μF, conduction-cooled, coil current:350A, frequency of coil current:16 kHz.

2.3 Test Setup

Electron Backscatter Diffraction (EBSD) analysis was executed utilizing a Zeiss Gemini SEM 300 model outfitted with Oxford's EBSD detector. Prior to analysis, sample preparation encompassed electropolishing using a solution consisting of 70% methanol, 20% perchloric acid, and 10% butanol, with a 20 V voltage applied for 20 seconds. The electropolishing procedure ensured a smooth and artifact-free surface for precise EBSD measurements. Subsequently, a dilution study was undertaken using a stereo-microscope (Zeiss Smartzoom-5) with 0.5x magnification. This study was conducted post-electropolishing and involved etching the sample with a 5% Nital solution. The combination of electropolishing and subsequent etching provided enhanced visibility and contrast for the examination of microstructural features during the EBSD analysis.

The assessment of residual stress was conducted using x-ray diffraction (XRD) testing, employing a PANalytical model (System-EMPYREAN). The experimental setup comprised a Cu target characterized by an average Kα wavelength of 1.5405 nm. A specific 2θ angle of 82.4° was selected for analysis, and the measurements were performed on the (2,1,1) crystallographic plane. The choice of these parameters in the XRD analysis was deliberate for accurate and precise evaluation of the residual stress within the material.

Vickers microhardness assessments were performed employing an Innovatest Model − 41 2D instrument. The specimens underwent meticulous polishing, and a 500gm load was applied for a duration of 10 seconds during the testing process. The microhardness testing was specifically conducted on the top surface of the specimens, and the analysis involved the determination of the average of three measured values to ensure a representative assessment of the material's hardness characteristics.

Miniature tensile test specimens, following the dimensions outlined in (Ref 25), were meticulously fabricated by precision

machining through wire-EDM from the sample as shown in Fig. 4(b). These specimens were characterized by a gauge length of 5 mm and a width of 2 mm. Subsequent to preparation, the specimens underwent mechanical testing utilizing the Tinius Olsen Model H25KS testing apparatus, with a controlled testing speed of 0.5 mm/min. The experimental setup, including the machine configuration and the loaded specimen, is visually represented in Fig. 5(a) and (b). The Tinius Olsen apparatus was chosen for its capacity to precisely measure the tensile properties of small-scale specimens. To ensure the reliability and consistency of the obtained results, three specimens were tested under each set of processing conditions as illustrated in Fig. 5(c), where the consistency across multiple tests for each processing condition is evident. The average values of these results were used for analysis.

3. Results and Discussion

3.1 Dilution

Dilution (or penetration) in AM is a key factor as it defines the bonding between two adjacent layers. There are various
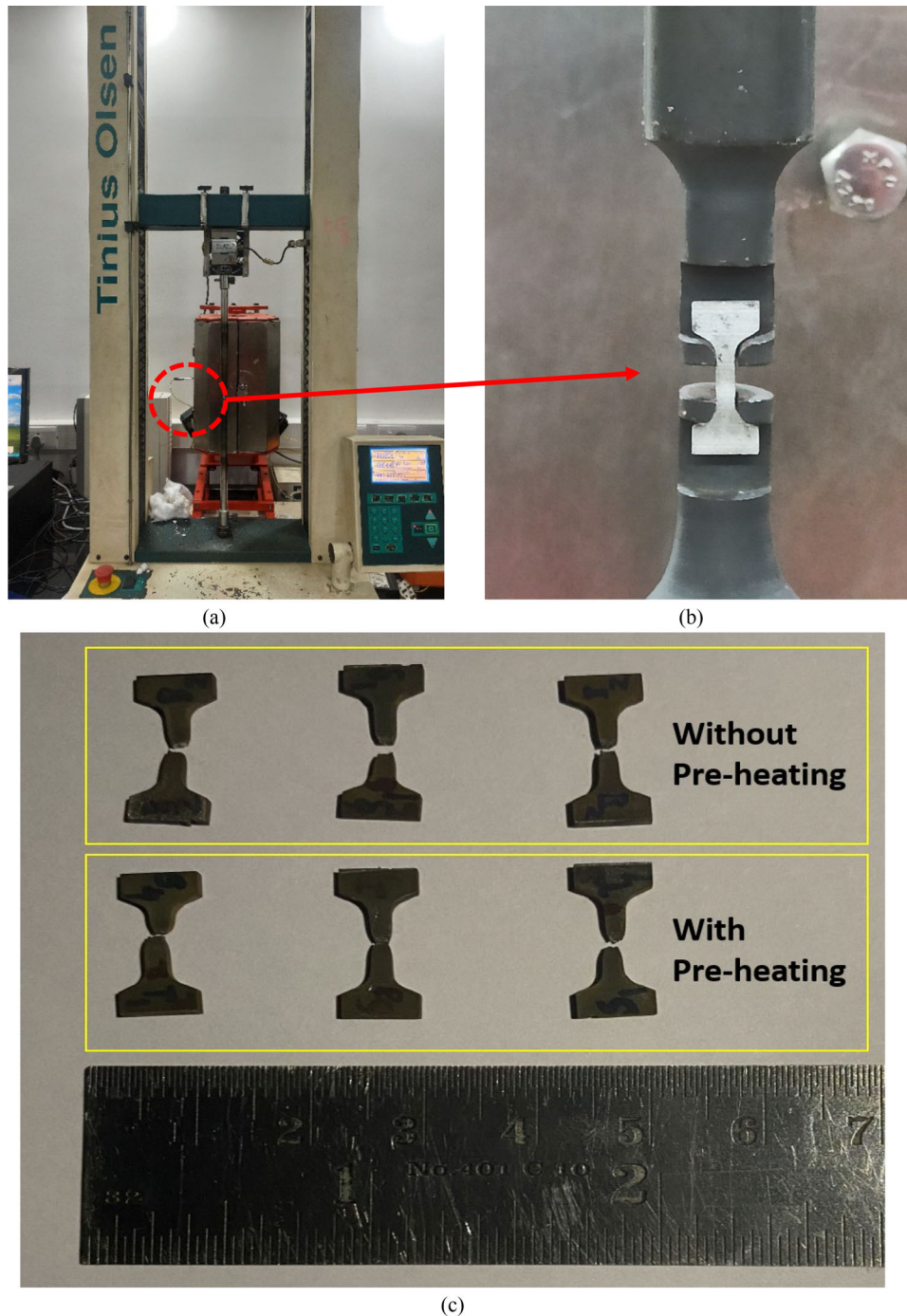

Fig. 5 (a) Tensile test setup; (b) Loaded tensile test specimen; (c) Broken test specimen

methods to increase the penetration by increasing the weld current/voltage or by decreasing the welding speed (Ref 26). In another study by Parveen et al. (Ref 27), it was found that effecting cooling behavior also increase the dilution with more heat input. Preheating as a parameter was studied by Satish et al. (Ref 28) and it was found that pre-heating temperature possess more effect on thermal gradient and plays vital role in bead profile and dilution along with other parameters like current, voltage, speed, etc. However, in our studies, the parameters were kept constant for all experiments and the effect of pre-heating are meticulously examined for WAAM process. Elevating the initial temperature of the base material through pre-heating results in a diminished thermal gradient. Consequently, when subjected to the high-temperature welding arc, a smaller temperature differential facilitates enhanced dilution of the new layer into the substrate or previously deposited material. Pre-heating additionally enables a gradual cooling process, as opposed to the rapid cooling observed in non pre-heated scenarios. This extended cooling period provides a more prolonged window during which the molten metal can effectively penetrate and fuse with the adjacent layer. The study of pre-heating on dilution reveals a stronger bond between layers. Initially the substrate dilution with single bead was examined and two samples were investigated: one without pre-heating and the other with pre-heating. It was observed that pre-heating resulted in increased dilution, attributed to enhanced fusion, as depicted in Fig. 6(a) & (b) with more homogeneous mixture between deposition and the substrate. In another study of multi-layer deposition, it was found that dilution between the layers was improved with pre-heating, the results are presented in Fig. 6 (c) & (d). The deposition was more uniform with pre-heating as depicted in Fig. 6 (d) which leads to stable deposition of subsequent layers.

The similar case was examined by Srinath et al. (Ref 14) for bead geometry investigation while depositing Inconel 625 on EN 8 steel, dilution was increased with the decrease in the height of deposition, however, a saturation was achieved with high heat input. Pre-heating in additive manufacturing modifies the thermal conditions of the substrate, making it more conducive to deep penetration by arc-based deposition. Dilution was enhanced in laser based deposition by more absorption in an induction-based pre-heating system of Co-based superalloys (Ref 15). Wang et al. (Ref 18) examined that with TIG arc-based pre-heating system the dilution was enhanced.

3.2 Grain Size and Orientation

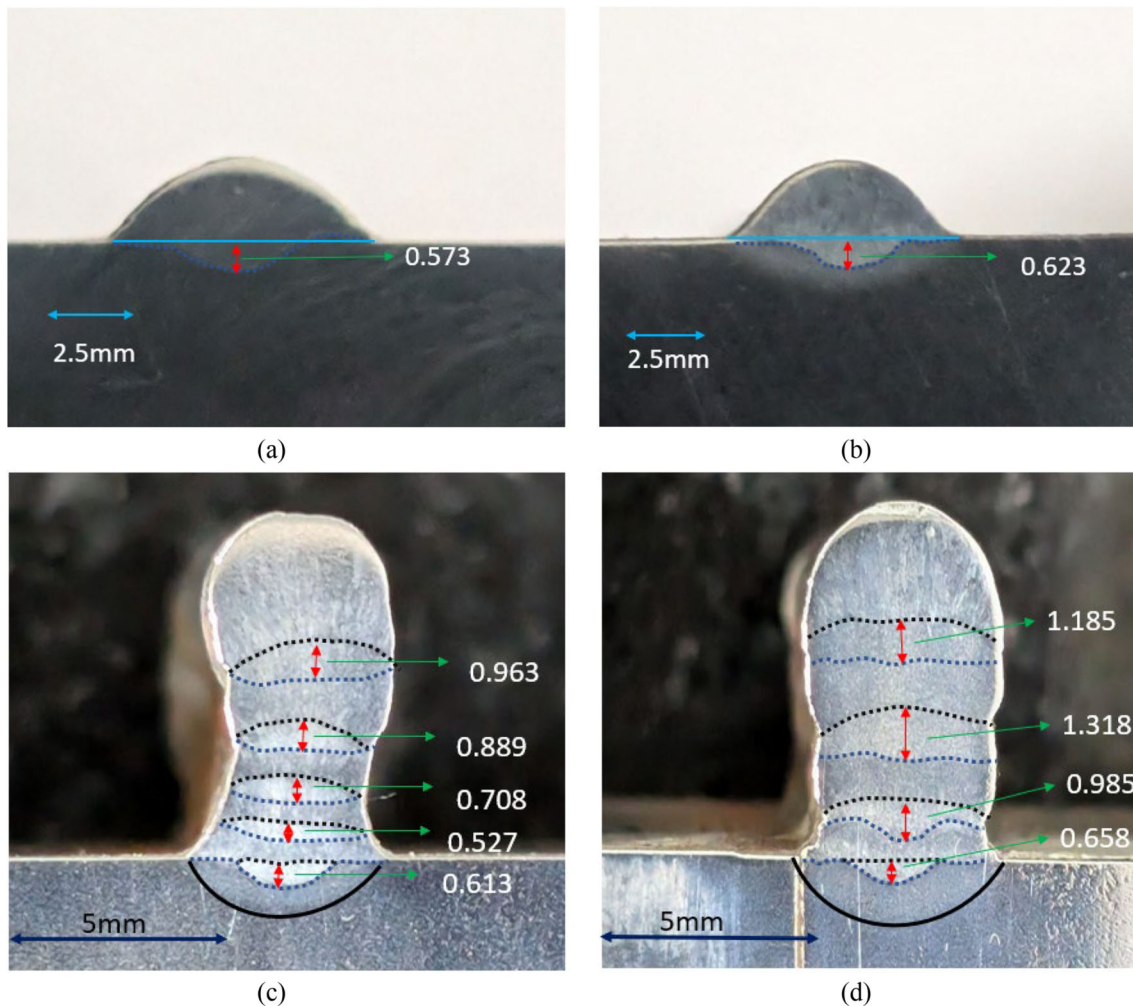The inverse pole figure map, derived from the Electron Backscatter Diffraction (EBSD) analysis, illustrates the grain

Fig. 6 Dilution with (a) substrate without pre-heating (b) substrate with pre-heating (c) interlayer without pre-heating (d) interlayer with pre-heating

size and orientation in the deposited condition with and without pre-heating, as depicted in Fig. 7. The EBSD scans were conducted over an area measuring $160 \times 160 \ \mu m$, employing a step size of 0.5 μm. Post-processing of the EBSD data was carried out using Aztech HKL software.

In the absence of pre-heating, the deposited sample exhibits a columnar grain structure, a consequence of its elevated heat input and directional solidification. Heat dissipates from the deposition area into the adjacent base material, prompting the metal to solidify in a directional manner. Typically, solidification initiates at the periphery and progresses toward the center, resulting in the formation of a columnar grain structure. The EBSD analysis provides a detailed visualization of these grain characteristics, offering insights into the microstructural features influenced by the welding process.

Induction pre-heating rapidly raises the material's temperature, 400 °C in 120 seconds in this case, fostering the development of a finer and more uniform microstructure with smaller grains due to the swift heating rate. Following the deposition, gradual cooling at ambient temperature facilitates a moderate cooling rate, thereby aiding in the development of a relatively refined microstructure. These accelerated heating and moderated cooling cycles restrain grain growth and reduce the average grain size. The shorter pre-heating time limits extensive recrystallization, impedes new grain formation, and prevents coarsening by reducing opportunities for grain growth (Ref 29, 30). It also constrains nucleation, resulting in a smaller grain size. Moreover, the pre-heating temperature influences the cooling rate, dictating the eventual grain size (Ref 31). As shown in Fig. 7, the grain size was compared for as-deposited (without pre-heat condition), and in pre-heating condition and it can be observed that most of the coarser grain structure (Fig. 7a) are refined (Fig. 7b).

The average grain size in as-deposited was found to be 13.82 μm, whereas in the case of the pre-heating sample, it was found to be 12.68 μm. This is mainly due to the reduction in the thermal gradient, which helps in a uniform cooling rate.

Zhou et al. (Ref 12) studied the effect of preheating on refining the structure of the deposited 24CrNiMoY alloy, and it was found that grain size reduced from 1.20 to 0.99 μm. Despite the formation of a coarser microstructure, pre-heating the substrate resulted in a more uniform structure in comparison to the condition where no pre-heating (cold substrate) was applied (Ref 32).

3.3 Residual Stress

Residual stresses arise because of strain incompatibility (Ref 33), which is caused due to three primary reasons: thermal variations, phase transformation, and mechanical processing. The deposition undergoes several thermal cycles during the formation of successive layers, which causes the residual stress buildup. Due to the thermal gradient mechanism as explained by Mercelis et al. (Ref 34) the rapid heating of the top surface and the development of a steep thermal gradient forcing the material to expand, however, the surrounding and underlying material restrains this expansion. The authors further expound on the cooling phase, wherein the top surface experiences a high solidification rate, leading to pronounced shrinkage. This shrinkage, once again, encounters restriction from the surrounding material, culminating in the manifestation of tensile residual stress on the top surface.

The material, while not undergoing plastic deformation, experiences multiple thermal cycles during the formation of successive layers, contributing to the gradual accumulation of tensile residual stresses on the top surface (Ref 35).

To investigate the residual stress on the top surface of the sample, an XRD test was performed and it was found that residual stress in the as-deposited block (without pre-heating) was 475 MPa in the x-direction and 411 MPa in the y-direction, and for the sample with pre-heating followed by deposition, the stresses in the x-direction were 220 MPa, and 253 MPa in the y-direction, the comparative result is presented in Fig. 8. Residual stresses are more in without pre-heated condition due to uneven cooling rate. Pre-heating results in more uniform thermal expansion and contraction due to decreased thermal gradient, thereby reducing residual stress. Its effect can be visualized by almost 50% reduction in residual stress values.

In another study by Mohsin et al. (Ref 35), a substantial decrease in residual stress values was observed when the cases were compared for as-deposited sample and with pre-heated sample for IN625 material. In a simulation work performed by Aggarangsi et at. (Ref 21), thermal gradient and maximum
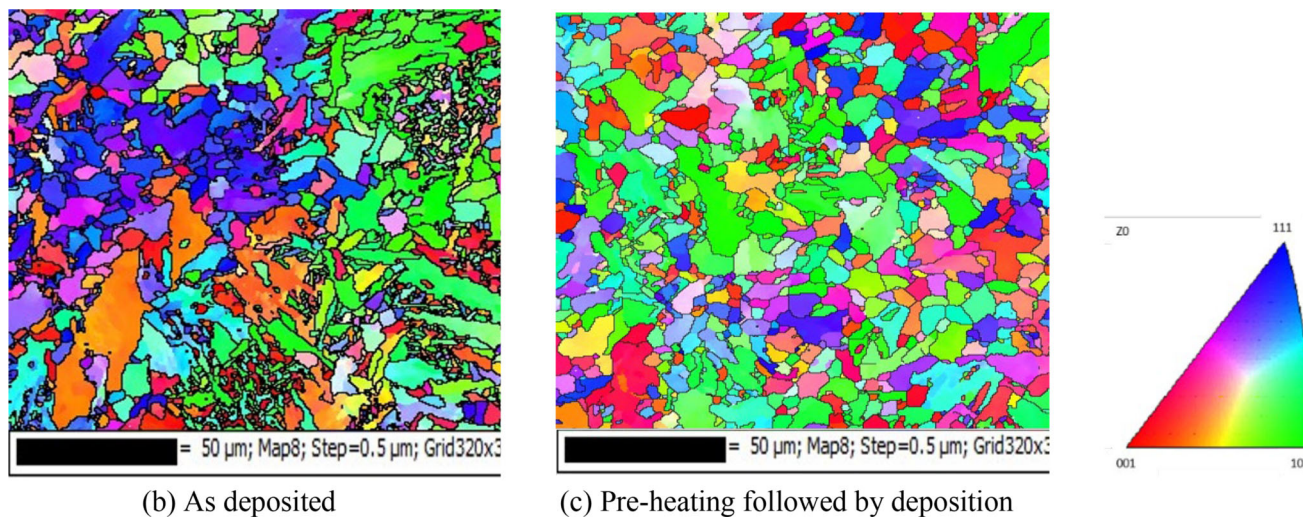

(b) As deposited

(c) Pre-heating followed by deposition

Fig. 7 IPF maps of different processing conditions

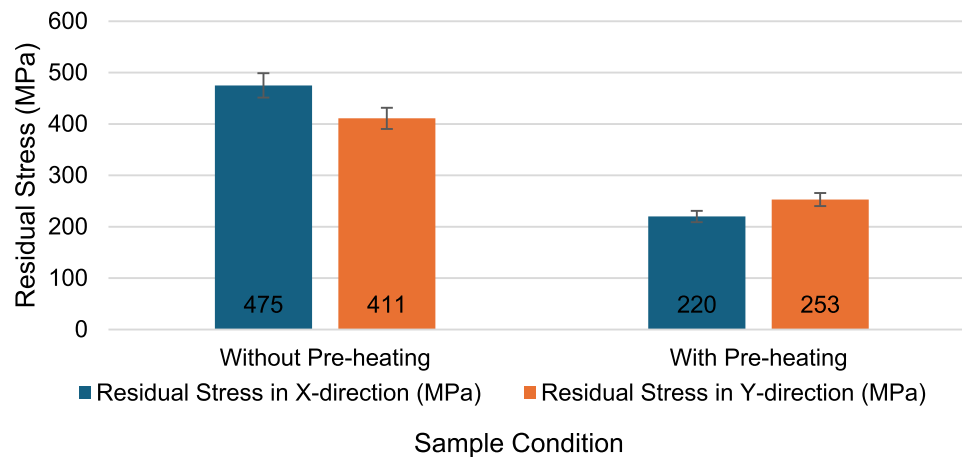## Effect of Pre-heating on Residual Stress

Fig. 8 Residual stress comparison of samples with and without pre-heating

stress were compared and 400°C temperature on top surface resulted in considerable low thermal gradient and substantial reduction in stress value.

3.4 Mechanical Properties: Tensile Strength & Micro Hardness

As a consequence of pre-heating, strong interlayer bonding is achieved, accompanied by grain refinement, leading to enhanced mechanical properties. As illustrated in Fig. 6, a visible improvement in dilution is evident, signifying enhanced fusion between the added layers and the substrate or previously deposited layers. This improvement is attributed to the elevated pre-heating temperature, which fosters superior metallurgical bonding. The elevated temperature facilitates a more thorough amalgamation of materials, resulting in an overall increase in the structural integrity of the component. The elevated pre-heating temperature plays a pivotal role in minimizing thermal stresses during the cooling phase. This reduction in thermal stresses results in a more homogeneous microstructure compared to as built condition as observed in Fig. 7. The uniformity in microstructural features contributes significantly to the improved tensile strength of the component. The interplay of improved dilution, enhanced metallurgical bonding, and reduced thermal stresses collectively underscores the beneficial impact of elevated pre-heating temperatures on the mechanical properties of the manufactured part. Tested samples exhibit sample without pre-heating has maximum ultimate tensile strength (UTS_{max}) of 537 MPa, and the sample with pre-heating results in 582 MPa, the comparative results are presented in Fig. 9 and the stress-strain mapping is presented in Fig. 10. The present results agree with increase in tensile strength value as presented in Pixner et at. (Ref 36). In another study of welding by Zhang et al. (Ref 29), a pre-heat temperature of 400 °C has significantly improved the tensile strength by 50% in Mo alloy.

The refinement observed in the grain structure resulting from pre-heating contributes to an augmentation in hardness. The maximum average hardness value for the as-deposited sample is measured at 146HV, whereas for the sample subjected

to pre-heating, it registers at 177HV. The hardness values along the build direction, explaining the disparity in hardness values, are graphically represented in Fig. 11. This increase in hardness is indicative of the influence of pre-heating on the microstructural characteristics and subsequent mechanical properties of the deposited material. Improvement in mean hardness was also attributed in 24CrNiMoY alloy samples when the samples were pre-heated at elevated temperature, and the hardness value increased from 354HV to 414HV (Ref 12). The top and bottom location exhibits higher values and top has comparatively more hardness, the similar trend was observed in the study of Anand et al. (Ref 37)

The hardness and UTS values depend on the average grain size as per the Hall-Petch equation, more refinement in grain structure improves this value further.

The hardness value in WAAM component usually varies from bottom to top layers due to different thermal cycles. The top layers has significant high hardness value and intermediate layers varies, similar trend was observed in the study of Tripathi et al. (Ref 38) and Anand et al. (Ref 37).

4. Conclusions

This paper addresses design and development of induction-based pre-heating setup compatible for WAAM process and evaluates its impact on material properties. This study compares the results of the samples with and without pre-heating and it has been found that pre-heating results in improved properties, following are the key conclusions:

- A 25 kW induction pre-heater was customized to meet specific application requirements, featuring dynamic power adjustments based on material composition and substrate size.
- The study's results indicate that pre-heating plays a pivotal role in significantly improving dilution, resulting in enhanced interlayer bonding in the deposition process.
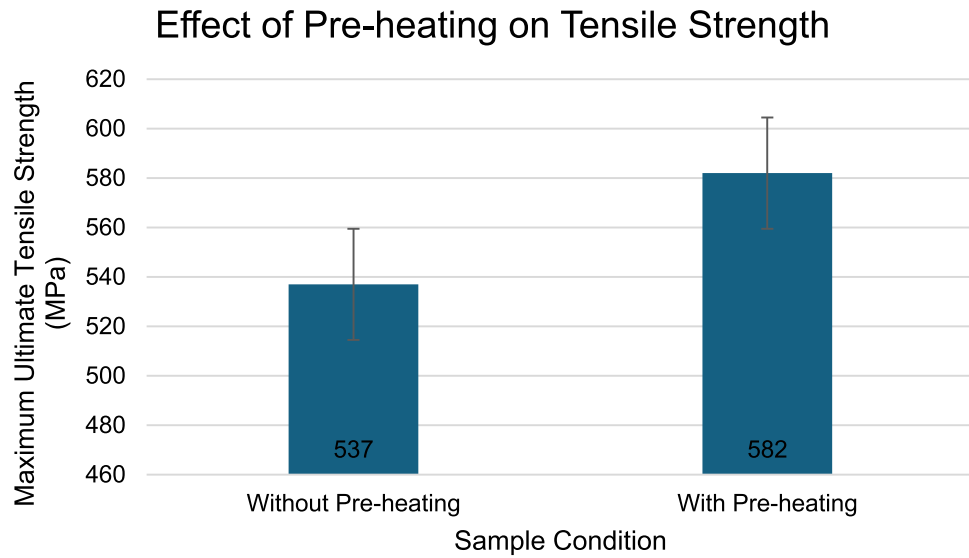
Fig. 9 Tensile strength comparison of samples with and without pre-heating
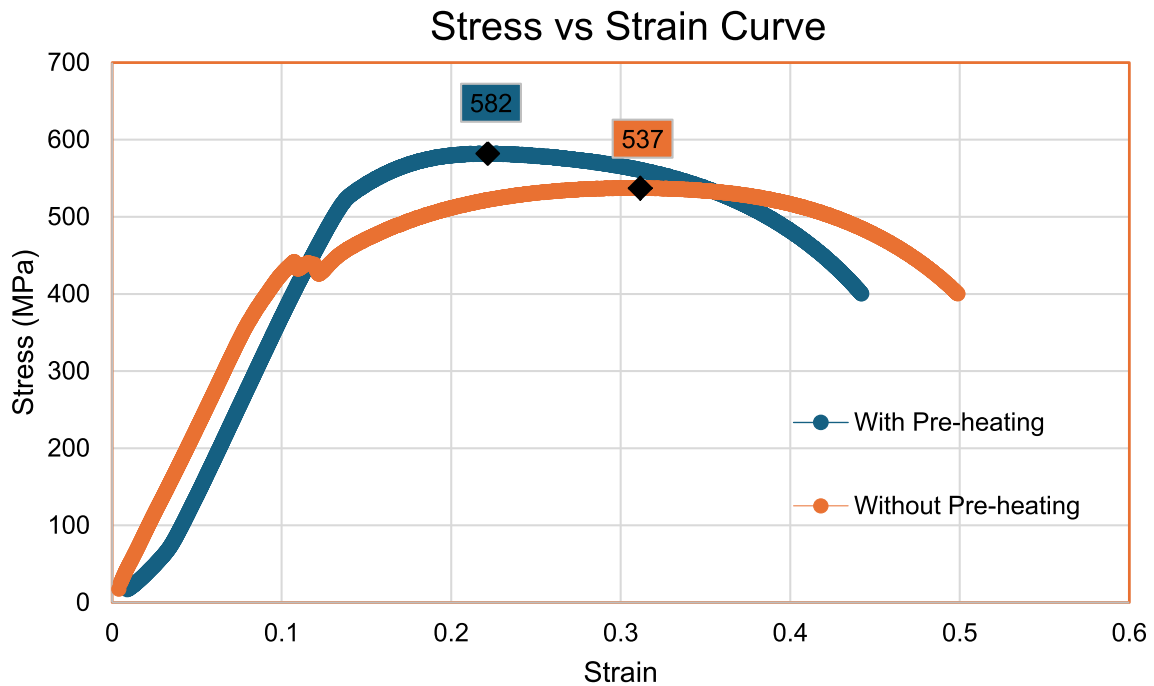

Fig. 10 Stress-strain curves for samples with and without pre-heating

- Furthermore, induction pre-heating contributes to the refinement of the grain structure, due to rapid heating followed by moderate rate of cooling during the solidification process. The grain size reduced from 13.82 (without pre-heating) to 12.68 μm (with pre-heating).
- As pre-heating also minimizes the thermal gradient, thus reduces the residual stress, the reduction in residual stress was almost 50%. Pre-heating also leads to uniform thermal cycles during repeating contraction and expansion.

- The refinement in grain sizes and improved interlayer bonding due to pre-heating causes improvement in mechanical properties; ultimate tensile strength experienced improvement from 537 to 582 MPa and hardness value increases from 146 to 177HV.
- The induction-based pre-heating system developed in this study demonstrates seamless compatibility with WAAM process, offering substantial advantages in achieving desired mechanical and metallurgical properties for addi-
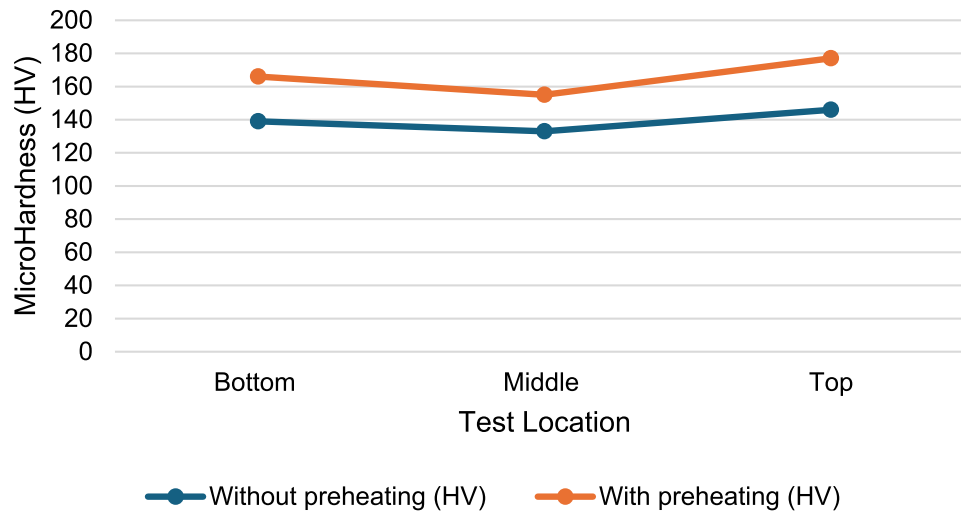
Hardness values along build direction

Fig. 11 Micro hardness comparison of samples with and without pre-heating

tively manufactured components. However, challenges still persist for the pre-heating of complex geometries.

References

1. K.P. Karunakaran, N. Kamal Gupta, A. Kumar Patel, K. Rakeshkumar, G. Ganesan, Siddhartha, M. Sealy, and A. Bernard, Multi-station multi-axis hybrid layered manufacturing (MSMA-HLM), *Manuf. Lett.*, 2022, **33**, p 630–639. https://doi.org/10.1016/j.mfglet.2022.07.078
2. J. Xiong, Y. Lei, and R. Li, Finite element analysis and experimental validation of thermal behavior for thin-walled parts in GMAW-based additive manufacturing with various substrate preheating temperatures, *Appl. Therm. Eng.*, 2017, **126**, p 43–52. https://doi.org/10.1016/j.applthermaleng.2017.07.168
3. M. Rauch, J.Y. Hascoet, and V. Querard, A multiaxis tool path generation approach for thin wall structures made with waam, *J. Manuf. Mater. Process.*, 2021, **5**(4), p 128
4. K. Lee and H. Jee, Slicing algorithms for multi-axis 3-D metal printing of overhangs, *J. Mech. Sci. Technol.*, 2015, **29**(12), p 5139–5144
5. N.K. Gupta, G. Ganesan, S. Siddhartha, S.R. Karade, S.D. Singh, and K.P. Karunakaran, A dual-side deposition technique to mitigate deformation in wire arc additive manufacturing. *Trans. Indian Inst. Met.,* 2024. https://doi.org/10.1007/s12666-024-03350-8
6. H. Shen, J. Lin, Z. Zhou, and B. Liu, Effect of induction heat treatment on residual stress distribution of components fabricated by wire arc additive manufacturing, *J. Manuf. Process.*, 2021, **2022**(75), p 331–345
7. C. Shang, C. Wang, C. Li, G. Yang, G. Xu, and J. You, Eliminating the crack of laser 3D printed functionally graded material from TA15 to Inconel718 by base preheating, *Opt. Laser Technol.*, 2020, **126**(December 2019), p 106100. https://doi.org/10.1016/j.optlastec.2020.106100
8. W. Meng, Y. Xiaohui, W. Zhang, F. Junfei, G. Lijie, M. Qunshuang, and C. Bing, Additive manufacturing of a functionally graded material from Inconel625 to Ti6Al4V by laser synchronous preheating, *J. Mater. Process. Technol.*, 2020, **275**, p 116368
9. X. Bai, H. Zhang, and G. Wang, Modeling of the moving induction heating used as secondary heat source in weld-based additive manufacturing, *Int. J. Adv. Manuf. Technol.*, 2015, **77**(1–4), p 717–727
10. L. Zhou, J. Sun, J. Chen, W. Chen, Y. Ren, Y. Niu, C. Li, and W. Qiu, Study of substrate preheating on the microstructure and mechanical performance of Ti-15Mo alloy processed by selective laser melting, *J. Alloys Compd.*, 2022, **928**, p 167130. https://doi.org/10.1016/j.jallcom.2022.167130
11. A.V. Müller, G. Schlick, R. Neu, C. Anstätt, T. Klimkait, J. Lee, B. Pascher, M. Schmitt, and C. Seidel, Additive manufacturing of pure tungsten by means of selective laser beam melting with substrate preheating temperatures up to 1000 °C, *Nucl. Mater. Energy*, 2019, **19**(February), p 184–188. https://doi.org/10.1016/j.nme.2019.02.034
12. L. Zhou, S. Chen, M. Wei, J. Liang, C. Liu, and M. Wang, Microstructure and properties of 24CrNiMoY alloy steel prepared by direct laser deposited under different preheating temperatures, *Mater CharactCharact.*, 2019, **158**(September), p 109931. https://doi.org/10.1016/j.matchar.2019.109931
13. M. Malý, K. Nopová, L. Klakurková, O. Adam, L. Pantělejev, and D. Koutný, Effect of preheating on the residual stress and material properties of Inconel 939 processed by laser powder bed fusion, *Materials (Basel)*, 2022, **15**(18), p 1–16
14. S. Gudur, V. Nagallapati, S. Pawar, G. Muvvala, and S. Simhambhatla, Materials today: proceedings a study on the effect of substrate heating and cooling on bead geometry in wire arc additive manufacturing and its correlation with cooling rate, *Mater. Today Proc.*, 2021, **41**, p 431–436. https://doi.org/10.1016/j.matpr.2020.10.071
15. Y. Hirono, T. Mori, M. Ueda, and D. Kono, Cracking suppression by substrate preheating using an induction heater in directed energy deposition, *J. Adv. Mech. Des. Syst. Manuf.*, 2023, **17**(3), p 1–15
16. E. Boudreault, B. Hazel, S. Godin, and J. Côté, A new robotic process for in situ heat treatment on large steel components, *Am. Soc. Mech. Eng. Power Div. POWER*, 2013, **2**, p 1–10
17. M. Gendron, B. Hazel, E. Boudreault, H. Champliaud, and X.T. Pham, Coupled thermo-electromagnetic model of a new robotic high-frequency local induction heat treatment system for large steel components, *Appl. Therm. Eng.*, 2019, **150**(December 2017), p 372–385
18. N. Wang, J. Shen, S. Hu, and Y. Liang, Numerical analysis of the TIG arc preheating effect in CMT based cladding of Inconel 625, *Eng. Res. Express*, 2020, **2**(1), p 015030
19. S. Raj and P. Biswas, Effect of induction preheating on microstructure and mechanical properties of friction stir welded dissimilar material joints of Inconel 718 and SS316L, *CIRP J. Manuf. Sci. Technol.*, 2023, **41**, p 160–179. https://doi.org/10.1016/j.cirpj.2022.12.014

20. A. Tiwari, P. Pankaj, S. Suman, P. Singh, P. Biswas, S. Pal, and A.G. Rao, Effect of plasma preheating on weld quality and tool life during friction stir welding of DH36 steel, *Proc. Inst. Mech. Eng. Part B J. Eng. Manuf.*, 2021, **235**(9), p 1458–1472

21. P. Aggarangsi and J.L. Beuth, Localized preheating approaches for reducing residual stress in additive manufacturing, *17th Solid Free. Fabr. Symp. SFF*, 2006, **2006**, p 709–720

22. A.K. Paul, Active-controlled passive distribution of power offers efficient heat treating solution for quality arc welding joints of steel pipes, *IEEE Trans. on Ind. Applicat.*, 2018, **54**(5), p 4958–4966

23. A.K. Paul, Zero-ventilated self-cooled induction heating device: topology and component engineering, *Power Electron. Devices Components*, 2022, **3**(July), p 100013. https://doi.org/10.1016/j.pedc.2022.100013

24. N. K. Gupta, G. Ganesan, Siddhartha, K. Shahu, A. K. Mehta, K.P. Karunakaran, Effect of multiple technologies on minimizing the residual stresses in additive manufacturing, in *ICRS 11 - The 11th International Conference of Residual Stresses, SF2M; IJL, Mar 2022, Nancy, France.*, 2022, https://hal.science/hal-04015039

25. K. Jacob, D. Yadav, S. Dixit, A. Hohenwarter, and B. Nagamani, Materials science & engineering a high pressure torsion processing of maraging steel 250: microstructure and mechanical behaviour evolution, *Mater. Sci. Eng. A*, 2021, **802**(December 2020), p 140665. https://doi.org/10.1016/j.msea.2020.140665

26. V.T. Le, Q. Thanh, D. Dinh, S. Mai, M. Cuong, B. Hoang, S. Tran, and X. Van Tran, Prediction and optimization of processing parameters in wire and arc - based additively manufacturing of 316L stainless steel, *J. Brazilian Soc. Mech. Sci. Eng.*, 2022, **44**(9), p 1–16. https://doi.org/10.1007/s40430-022-03698-2

27. P. Kumar, S. Kumar, S. Ratnesh, and K. Raj, Effect of cooling media on bead geometry, microstructure, and mechanical properties of wire arc additive manufactured IN718 alloy, *Adv. Manuf.*, 2024, **12**(1), p 124–149. https://doi.org/10.1007/s40436-023-00457-x

28. S.K. Sharma, S. Maheshwari, R. Kumar, and R. Singh, Effect of Heat-Input and Cooling-Time on Bead Characteristics in SAW, *Mater. Manuf. Process.*, Taylor & Francis, 2019, **34**(2), p 208–215, https://doi.org/10.1080/10426914.2018.1532578

29. L.J. Zhang, J.Z. Liu, Q.L. Bai, X.W. Wang, Y.J. Sun, S.G. Li, and X. Gong, Effect of preheating on the microstructure and properties of fiber laser welded girth joint of thin-walled nanostructured Mo alloy, *Int. J. Refract. Met. Hard Mater.*, 2019, **78**(April 2018), p 219–227

30. A. Mostafapour, H. Vahedi, and A. Ebrahimpour, Experimental study on the effects of preheating time and temperature of hot press process on the mechanical and metallurgical properties of AZ91C alloy sheet, *Mater. Res. Express*, 2019, **6**(5), p 056562

31. J. Wang, X. Chen, L. Yang, and G. Zhang, Effect of preheat & post-weld heat treatment on the microstructure and mechanical properties of 6061–T6 aluminum alloy welded sheets, *Mater. Sci. Eng. A*, 2022, **841**(July 2021), p 143081

32. S.K. Moheimani, L. Iuliano, and A. Saboori, The role of substrate preheating on the microstructure, roughness, and mechanical performance of AISI 316L produced by directed energy deposition additive manufacturing, *Int. J. Adv. Manuf. Technol.*, 2022, **119**(11–12), p 7159–7174. https://doi.org/10.1007/s00170-021-08564-4

33. D. Zaza, M. Ciavarella, and G. Zurlo, Strain incompatibility as a source of residual stress in welding and additive manufacturing, *Eur. J. Mech. A/Solids*, 2021, **85**, p 104147. https://doi.org/10.1016/j.euromechsol.2020.104147

34. P. Mercelis and J.P. Kruth, Residual stresses in selective laser sintering and selective laser melting, *Rapid Prototyp. J.*, 2006, **12**(5), p 254–265

35. K. MohsinKhan, T.B. Rao, B.N. Manjunath, K. Abhinav, A.R. Vinod, and R. Mohammed, Studies on the effect of substrate preheating, interlayer dwell, and heat treatment on microstructure, residual stress, and mechanical properties of IN625 superalloy built by direct metal deposition, *J. Eng. Mater. Technol.*, 2023 https://doi.org/10.1115/1.4062503

36. F. Pixner, R. Buzolin, F. Warchomicka, M. Dománková, M. Čaplovičová, F. Riedlsperger, S. Fritsche, M. Orłowska, J. Domitner, M. Lasnik, and N. Enzinger, Influence of process and heat input on the microstructure and mechanical properties in wire arc additive manufacturing of hot work tool steels, *Mater. Sci. Eng. A*, 2023, **888**(December 2022), p 145799

37. M. Anand, H. Bishwakarma, N. Kumar, K. Ujjwal, and A. Kumar Das, Fabrication of multilayer thin wall by WAAM technique and investigation of its microstructure and mechanical properties, *Mater. Today: Proc.*, 2022, **56**, p 927–930

38. U. Tripathi, N. Saini, R.S. Mulik, and M.M. Mahapatra, Effect of build direction on the microstructure evolution and their mechanical properties using GTAW based wire arc additive manufacturing, *CIRP J. Manuf. Sci. Technol.*, 2022, **37**, p 103–109. https://doi.org/10.1016/j.cirpj.2022.01.010